

Proton Computed Tomography reconstruction using a backprojection-then-filtering approach

G Poludniowski^{1‡}, N M Allinson² and P M Evans¹

¹ Centre for Vision Speech and Signal Processing, University of Surrey, Guildford, GU2 7XH, UK

² Laboratory of Vision Engineering, School of Computer Science, University of Lincoln, Lincoln, LN6 7TS, UK

E-mail: g.poludniowski@surrey.ac.uk

Abstract. A novel approach to proton CT reconstruction using backprojection-then-filtering is proposed. A list-mode algorithm is formulated accommodating non-linear proton paths. The analytical form is derived for the deblurring kernel necessary for the filtering step. Further, a finite matrix correction is derived to correct for the limited size of the backprojection matrix. High quantitative accuracy in relative stopping power is demonstrated ($\leq 0.1\%$) using Monte Carlo simulations. This accuracy makes the algorithm a promising candidate for future proton CT systems in proton therapy applications. For the purposes of reconstruction, each proton path in the object-of-interest was estimated based on a cubic spline fit to the proton entry and exit vectors. The superior spatial-resolution of the backprojection-then-filtering (BPF) method over the standard filtering-then-backprojection (FBP) approach is demonstrated. As the BPF algorithm requires only one backprojection and filtering operation on a scan data set, it also offers computational advantages over an iterative reconstruction approach.

PACS numbers: 87.57.Q-, 87.57.nf

Submitted to: *Phys. Med. Biol.*

1. Introduction

The utility of imaging with protons instead of x-rays for proton therapy is an old idea that has recently received renewed interest. Cormack, over fifty years ago, considered performing Computed Tomography (CT) with protons to reconstruct stopping-power and obtain increased accuracy in treatment planning (Cormack 1963). He foresaw a fundamental difficulty: the statistical variations in the path and energy (or “straggling”) of protons after having passed through a given thickness of tissue. This difficulty did not prove insurmountable, and the principle was subsequently demonstrated experimentally (Cormack and Koehler 1976, Hanson *et al* 1978). Hanson proposed the incorporation

‡ Currently also a Visiting Scientist at the Department of Medical Physics, Karolinska University Hospital, 171 76 Stockholm, Sweden.

of non-linear approximations to proton trajectories within the reconstruction (Hanson 1979) and a literature has built up on this topic (Schneider and Pedroni 1994, Williams 2004, Schulte *et al* 2008, Wang *et al* 2010). Motivated by the potential application in proton therapy planning, a number of research groups have contributed to developments in proton radiography in recent years (e.g. Schneider *et al* 2004, Civinini *et al* 2010, Sadrozinski *et al* 2013, Poludniowski *et al* 2014). There is also a small but growing body of research addressing the fundamental question of the CT reconstruction itself (Penfold *et al* 2009, Penfold *et al* 2010, Cirrone *et al* 2011, Rit *et al* 2013).

The canonical way to do CT reconstruction has for a long time been by the Filtered Backprojection (FBP) approach (Kak and Slaney 2001). This consists of:

- (i) Uniformly sampling ray-projections through a 2D slice of a body with a detector;
- (ii) Convoluting this array of data with a 1D kernel (or equivalently filtering in the spatial-frequency domain);
- (iii) Backprojecting the convolved ray-projections through a 2D reconstruction matrix;
- (iv) Repetition over a set of angles of orientation.

A complete volume (or voxel set) is built up out of a series of 2D slices. The elegance and economy of the approach have led to its dominance and it is still the primary method for reconstruction in hospital CT systems, although iterative/statistical methods of reconstruction are gaining ground (Beister *et al* 2012).

To obtain optimal spatial resolution in proton CT, it is now understood that it is necessary to measure the properties of each proton that passes through an object and to incorporate non-linear estimates of each proton's trajectory into the reconstruction (Li *et al* 2006). These two points, the list-mode nature of the data and the non-parallel and non-linear proton paths, puts into question the suitability of the whole FBP method. Indeed a number of authors have instead chosen iterative strategies and accepted the greatly increased computational burden that accompanies the power of that approach (see e.g. Penfold *et al* 2010). However, if FBP is pursued, a choice of how to bin the data must be made so that it can be filtered. Some authors have made the decision to apply strict cuts to eliminate large deviations from straight paths, at the cost of increasing imaging dose for the same number of useful protons (Cirrone *et al* 2011). The approach of performing a voxelwise rebinning of data has also been suggested and produced encouraging results (Rit *et al* 2013), but would necessitate substantially increased complexity and computation.

Yet the FBP approach is not the only analytic approach to tomographic reconstruction. An alternative approach of Backprojection-then-Filtering (BPF) is proposed here and it is argued that this method more naturally fits the nature of the problem. The quantitative accuracy of the BPF approach is demonstrated after the application of suitable corrections for the finite size of the backprojection matrix.

2. Method

2.1. Backprojection-then-filtering

Both FBP and BPF are analytic techniques in that they solve the problem of going from the radon transform of an object (the measurements) to the reconstructed object (the 2D image slice) using each datum only once. The approach of Backprojection Filtering (BPF) has long been known (Suzuki and Yamaguchi 1988) but rarely used. The approach consists of:

- (i) Sampling ray-projections through a 2D slice (not necessarily uniformly);
- (ii) Backprojecting the ray-projections through a 2D reconstruction matrix;
- (iii) Convoluting (or filtering) this 2D matrix of data with a 2D kernel;
- (iv) Repetition over a set of angles of orientation.

The reordering of the filtering and backprojection operations between FBP/BPF approaches may appear trivial but has profound consequences. FBP has generally been preferred over BPF for a number of reasons (Zeng and Gullberg 1994, Zeng and Gullberg 1995). Firstly, the filtering operation in BPF is in 2D and therefore requires more computation and computer memory. Secondly, analytic results for BPF convolution kernels are more difficult to obtain. Thirdly, the BPF approach has had issues with quantitative accuracy. With modern computing power, the somewhat increased computational demand of using 2D Fourier transforms in BPF is not a substantial issue. The second and third points are important but novel contributions to dealing with these are described here. The question remains, why should we ever use BPF at all in preference to FBP? We suggest the following advantages for the proton CT problem: BPF naturally deals with list-mode data (one particle at a time) without the need for binning and it can naturally accommodate non-linear ray-projection paths. Because the filtering operation occurs after the backprojection of each proton path onto a regular matrix in image space, the binning requirement of FBP is completely side-stepped.

2.2. Mathematical formulation of BPF

Suppose a 2D slice of a body has some property described by the function, $f(x, y)$, which is zero outside some region, Ω_f . In the case of proton CT the appropriate property is proton relative stopping-power (RSP). A line integral through the body, at an angle, ϕ , and displacement, t (see Fig. 1), can be written as,

$$p(t, \phi) = \int dx dy f(x, y) \delta(x \cos \phi + y \sin \phi - t). \quad (1)$$

This line integral is a ray-projection through the body slice and is related to Water-Equivalent-Path-Length (WEPL). The transform from the space (x, y) to (ϕ, t) is the Radon transform.

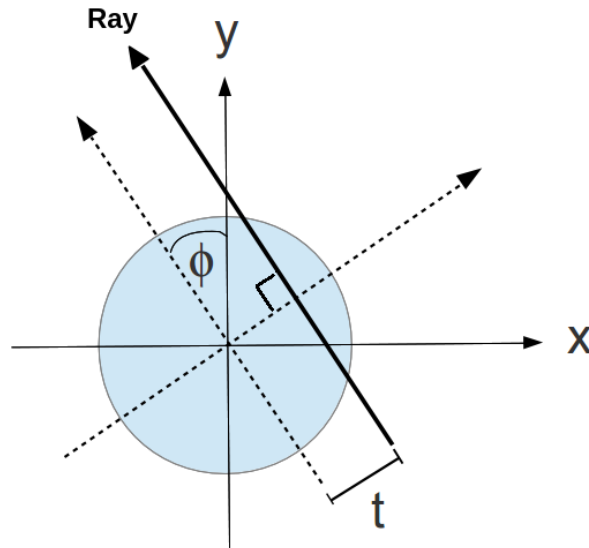


Figure 1: Illustration of Radon transform geometry.

The backprojection operation is defined as,

$$b(x, y) = \int dt d\phi p(t, \phi) \delta(x \cos \phi + y \sin \phi - t) \quad (2)$$

$$= \int_0^\pi d\phi p(t, \phi) |_{x \cos \phi + y \sin \phi = t} \quad (3)$$

This is equivalent to tracing back along the ray-projection path and depositing at each location that it passes through the value of the line-integral. The resulting backprojection function, $b(x, y)$, resembles a blurred-out representation of the density function, $f(x, y)$. In fact they are related by (Zeng and Gullberg 1994),

$$b(x, y) = f(x, y) ** \frac{1}{r}, \quad (4)$$

where $**$ denotes a 2D convolution and $r = \|(x, y)\|$. Note that even though we required $f(x, y)$ to be zero outside the region Ω_f , the function $b(x, y)$ is non-zero everywhere.

The convolution relation can be expressed as a filtering operation in 2D Fourier space. Forward and inverse Fourier transforms will be indicated by $\mathcal{F}\{\dots\}$ and $\mathcal{F}^{-1}\{\dots\}$, respectively. Let the Fourier conjugate variables to (x, y) be (u, v) and $\rho = \|(u, v)\|$. Then we can write:

$$f(x, y) = \mathcal{F}^{-1} \left\{ \frac{\mathcal{F}\{b\}}{\mathcal{F}\{r^{-1}\}} \right\} = \mathcal{F}^{-1} \{ \mathcal{F}\{b\} \rho \} \equiv b(x, y) ** k(x, y), \quad (5)$$

where $k(x, y)$ is a spatial kernel. The following result (valid for 2D Fourier transforms) has also been used: $\mathcal{F}\{r^{-1}\} = \rho^{-1}$.

2.3. The backprojection operation

For practical implementation in an algorithm, a discretized formula for the backprojected image, b , needs to be used. The 2D matrix for b can be calculated from

acquired measurements in a number of ways. Imagine that projections are acquired at a set of discrete rotation angles, $\phi_l = \pi \frac{l-1}{L}$ where $l \in \{1, 2, \dots, L\}$. At each angle, K ray-projections are sampled (not necessarily uniformly) over the field encompassing the object with each ray designated an index, $k \in \{1, 2, \dots, K\}$. This provides a discretized radon transform matrix, $p[k, l]$. Now consider a discrete 2D backprojection matrix, $b[i, j]$, with corresponding pixel centres $x_i = (2i - N - 1)\tau/2$ and $y_j = (2j - N - 1)\tau/2$. Here, τ is the matrix pitch and $i \in \{1, 2, \dots, N\}$ and $j \in \{1, 2, \dots, N\}$. The backprojection matrix can be expressed in terms of the discrete radon transform as follows:

$$b[i, j] = \frac{\pi}{L} \sum_{l=1}^L \frac{\sum_{k=1}^K \lambda_{k,l}[i, j] p[k, l]}{\sum_{k=1}^K \lambda_{k,l}[i, j]}, \quad (6)$$

where $\lambda_{k,l}[i, j]$ is the path length of the k th ray of the l th projection through the pixel $[i, j]$.

2.4. The filtering operation

Two observations should be made at this point. Firstly, by selecting a sampling pitch for backprojection the convolution kernel becomes band-limited in spatial-frequency. Secondly, a finite matrix size must be chosen for the kernel. To acquire quantitatively accurate results, the band-limit due to sampling pitch must be imposed on the filter in the frequency domain and then the resulting spatial kernel sampled on a finite matrix in the spatial domain. If this procedure is not followed an almost constant shift in all the reconstructed values results (Zeng and Gullberg 1995).

The band-limit on spatial-frequencies is imposed by modifying the ramp (or ‘‘rho’’) filter representation of the kernel in frequency space:

$$K(\rho) = \rho \quad \text{if } \rho < (2\tau)^{-1} \quad (7)$$

$$= 0 \quad \text{otherwise} \quad (8)$$

This is exactly as is done in the classic Filtered Backprojection (FBP) algorithm with one important difference: the relationship between the convolution kernel and filter involves a 2D *not* a 1D Fourier transform. This renders the analytic evaluation more difficult as remarked by Zeng and Gullberg (1995). In fact, we were unable to find the analytic form of the 2D spatial kernel, $k(r)$, in the literature. However, it can be obtained as follows:

$$k(r) = \mathcal{F}^{-1}\{K(\rho)\} \quad (9)$$

$$= \int_0^{1/2\tau} \rho d\rho \int_{-\pi}^{\pi} d\phi \rho e^{j2\pi\rho r \cos(\theta-\phi)} \quad (10)$$

$$= 2\pi \int_0^{1/2\tau} d\rho \rho^2 J_0(2\pi r \rho) \quad (11)$$

$$= \frac{1}{4\pi^2 r^3} \left[\left(\frac{\pi r}{\tau} \right)^2 J_1 \left(\frac{\pi r}{\tau} \right) - \Phi \left(\frac{\pi r}{\tau} \right) \right], \quad (12)$$

where

$$\Phi(x) = \frac{\pi x}{2} [J_1(x)H_0(x) - J_0(x)H_1(x)], \quad (13)$$

and J_n and H_n are n th order Bessel and Struve functions, respectively. The integral over ϕ was performed using an integral definition of the Bessel function (Jeffrey and Zwillinger, 2010). The integral over ρ was performed using a known integral identity (Rosenheinrich 2013). The fact that the analytic expression for the kernel can only be expressed in terms of special functions is inconvenient, but not problematic, since fast library routines for calculating these functions are available. Note, for implementation purposes, that despite the divergent pre-factor of r^{-3} in the above equation, the kernel remains finite at zero:

$$k(r)|_{r=0} = \frac{\pi}{12\tau^3}. \quad (14)$$

The finite size of the backprojection matrix and kernel must also be considered to find the appropriate filter in discrete Fourier space. The correct filter to use is a Discrete Fourier Transform (DFT) of the finite band-limited kernel we have just derived. The filtering operation is then performed by the following:

$$f[i, j] = DFT^{-1} \{DFT\{b[i, j]\}DFT\{k[i, j]\}\}, \quad (15)$$

with appropriate zero-padding (where DFT^{-1} is the inverse transform). An additional smoothing filter e.g. Shepp-Logan or Gaussian can safely be applied by sampling the appropriate function in the frequency domain and multiplying the kernel filter by it in equation 15. In this case, since any well-designed smoothing filter should leave the low-spatial frequency components unchanged, it is not necessary to find the band-limited kernel of the smoothing filter and then apply a DFT.

2.5. Finite matrix correction

The mathematical formulation outlined above described the BPF process and how to implement it. However, if you follow the suggested recipe you still may not reconstruct quantitatively accurate images of proton stopping power at the one percent level. In practice, a finite region, Ω_b , must be chosen for the backprojection. This is a problem, because the blurred-out function $b(x, y)$ is non-zero everywhere and the data truncation leads to quantitative inaccuracy (Suzuki and Yamaguchi 1988).

Previously, it seems, the only attempt to deal with this has been to make the discretized backprojection matrix ($N \times N$) finite but much larger than the desired image matrix ($M \times M$). This is expensive in computer memory and computation time, as well as only asymptotically improving accuracy.

The effect of missing data due to a finite backprojection matrix, closely resembles a constant offset in the reconstructed function, $f(x, y)$. After all, the effect of distant data on the reconstruction region *can* only manifest in the low-spatial frequencies. A constant-shift correction can be arrived at in a number of ways. Consider the following.

We can write the backprojection function as a convolution (see equation 4),

$$b(x, y) = f(x, y) * * \frac{1}{r} = \int_{\in \Omega_f} dx' dy' \frac{f(x', y')}{\sqrt{(x - x')^2 + (y - y')^2}}. \quad (16)$$

The distant values of the backprojection matrix, if far enough away from the central region, can then be approximated as:

$$b_{r \gg r'}(x, y) \approx \frac{1}{r} \int_{\in \Omega_f} dx' dy' f(x', y'). \quad (17)$$

The contribution to $f(x, y)$ of the missing data, is therefore approximately (see equation 5):

$$\begin{aligned} \Delta(x, y) &= \int_{\notin \Omega_b} dx' dy' b_{r \gg r'}(x', y') k(x - x', y - y') \\ &= \left(\int_{\in \Omega_f} dx' dy' f(x', y') \right) \left(\int_{\notin \Omega_b} dx' dy' \frac{k(x - x', y - y')}{r'} \right). \end{aligned} \quad (18)$$

It should be understood that the integral inside the first brackets is over all points in the reconstruction region ($\in \Omega_f$) while that inside the second brackets is over all points *outside* the backprojection region ($\notin \Omega_b$). To the central pixel, [$i = N/2, j = N/2$], the correction becomes:

$$\Delta = \left(\tau^2 \sum_{\text{pixels} \in \Omega_f} f[i, j] \right) \left(\tau^2 \sum_{\text{pixels} \notin \Omega_b} \frac{k[N/2 - i, N/2 - j]}{\tau \sqrt{i^2 + j^2}} \right). \quad (19)$$

The second sum over all pixels outside the backprojection matrix is in principle an infinite sum, but can be evaluated inexpensively to the desired accuracy. This correction, Δ , calculated for one pixel, should then be applied to *all* pixels in the image as a constant offset:

$$f_{\Delta}[i, j] = f[i, j] + \Delta. \quad (20)$$

2.6. Relaxation of the 2D conditions

It should be noted that the above formulation for reconstruction assumes linear in-plane ray-projections (in this case proton paths). As such, each slice of the 3D volume should factorize into a separate 2D problems with distinct data. This is the essence of classical tomography. In reality, due to beam angular dispersion and straggling, protons will not typically remain in the same axial plane as they progress through the patient. However, both the angular dispersion and straggling of protons is typically small enough to be considered a perturbation. Typical root-mean-square figures for beam divergence before and after the patient might be 5 mrad and 50 mrad respectively (Bruzzi *et al* 2007), although these values would depend on the beam nozzle design, proton energy and size of patient. We therefore propose the following adaptation to non-linear out-of-plane paths. Firstly, the backprojection is performed as expressed in equation 6, except that ray paths are backprojected along non-linear trajectories through the 3D volume and

may pass through multiple axial slices. Secondly, the filtering operation, as described in equation 15, is performed slice by slice as if the protons had progressed linearly, parallel and in-plane.

2.7. Simulations

To demonstrate the proposed algorithm, a simulation of a proton CT scan acquisition was performed using the FLUKA Monte Carlo code (Ferrari *et al* 2005) and FLAIR interface (Vlachoudis 2009). The test object was a variant of the 3D Shepp-Logan head phantom (Kak and Slaney 2001) consisting of twelve regions constructed from ten ellipsoids. The phantom was scaled to give maximum thicknesses in the x, y and z directions of 13.8, 18.4 and 18.0 cm, respectively. All the regions were modelled as water, but assigned densities between 1.00 and 2.00 g·cm⁻³, with the background density set as 1.02 g·cm⁻³. Additionally, a tungsten bar (diameter: 0.5 mm) was inserted into the phantom to allow quantification of the Modulation-Transfer-Function (MTF).

The source was modelled as a 10 cm diameter parallel and mono-energetic beam of 200 MeV protons (initial kinetic energy). The entry and exit four-vectors of each proton were scored at planes parallel to the beam axis, located at 12 cm from the isocentre. The scoring was implemented using a user-modified version of the *mgdraw* routine supplied with FLUKA§. A total of 180 projections were simulated equally spaced over π radians, each projection consisting of 10⁷ primary protons. The dose to the centre of the phantom was recorded using the USBIN scoring card. Only protons which emerged from the phantom in the forward direction were considered usable. In addition, during post-processing of the FLUKA output, cuts were applied in angular and lateral deflection at the exit plane using 0.5x0.5 mm² scoring zones. This was implemented to eliminate events likely to involve inelastic nuclear interactions and to limit the blurring effect of straggling. Sequentially, a 3 σ then a 2 σ cut were applied for these purposes in each lateral direction. After particle loss and rejection, approximately 83% of the initial protons remained for reconstruction. The Water-Equivalent-Path (WEPL) for each proton was then calculated by subtracting the residual range of the proton at the exit plane from its initial range, using the NIST tabulations of proton range (Berger *et al* 2005).

2.8. Implementation of proposed BPF algorithm

The BPF algorithm proposed above was implemented in Fortran 95/2003 and compiled with the gfortran compiler. The OpenMP library of gfortran was used to allow multi-threaded execution. The 2D Fourier Transforms were implemented using the external FFTW3 library||. The Struve functions were calculated using the external *special_functions* Fortran 90 library, derived from Zhang and Jin¶. Backprojection

§ See the FLUKA online manual at: www.fluka.org

|| See: <http://www.fftw.org/>

¶ See: http://people.sc.fsu.edu/~jburkardt/f_src/special_functions/special_functions.html

was performed on a $N \times N \times L$ matrix of voxels. Reconstructed stopping-powers were calculated on a $M \times M \times L$ matrix. Unless otherwise indicated, 1 mm^3 voxels were used for reconstruction ($M=L=200$) and a 2D Gaussian smoothing filter was applied ($\sigma = 1/\sqrt{2}$ pixels). The backprojection matrix was oversized by a factor of either two ($N = 2M$) or four ($N = 4M$).

Reconstructions for the determination of Modulation-Transfer-Functions (MTFs) were performed at higher resolution ($N=4M=8L=1600$, $0.5 \times 0.5 \times 1.0 \text{ mm}^3$ voxels, no Gaussian filter applied). The MTF determination followed that recommended for the Catphan phantom⁺. Note that no correction for the finite size of the tungsten bar was applied.

The backprojection operation was ray-driven on a history by history basis, applying equation 6. Inside the phantom, for each proton, n knot points were calculated equally spaced between the phantom entry and exit points. These points sat on a cubic spline trajectory estimated from the proton's entry and exit vectors (Williams 2004). Inside the phantom, backprojection was linear between any two knot points (see figure 2). Outside the phantom, the protons were projected back from the surface with trajectories parallel to the beam axis (at an angle ϕ in the x-y plane). This stops the backprojection rays "spreading-out" as they diverge from the phantom which would exacerbate the departures from the ideal case discussed in Section 2.6. Backprojecting away from the phantom into empty space along the actual entry and exit trajectories was found to lead to a small quantitative error in reconstructed stopping powers of up to 1%.

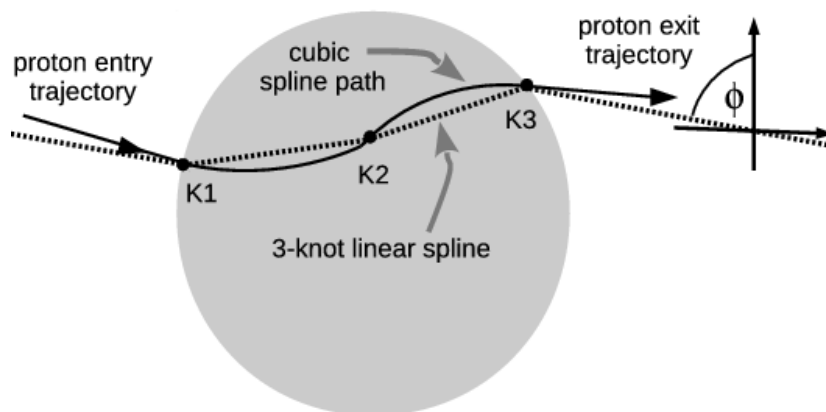


Figure 2: Illustration of a linear spline approximation to proton trajectory (dotted path) in comparison to a cubic spline estimate (solid path). A 3-knot linear spline is depicted.

2.9. Implementation of a standard FBP algorithm

To compare the proposed BPF algorithm to a more conventional approach, a version of a FBP algorithm was implemented. This is termed standard FBP here (SFBP), because

⁺ See the Catphan 500 and 600 manual (The Phantom Laboratory): <http://www.phantomlab.com/products/catphan.php>.

we take the most natural implementation. For each of the 180 projections, the WEPLs of the protons were binned to a 2D matrix at the exit plane, enabling filtering prior to backprojection. The pixel size for this binning was chosen as 0.5 mm. The projections were then filtered with the appropriate 1D ramp filter and backprojected assuming rays parallel to the beam axis. In this formulation, the use of an approximation to curved proton trajectories was not possible. For the same event-rejection cuts applied to the exit trajectories, the FBP algorithm would therefore be expected to result in poorer spatial resolution compared to the BPF approach. Reconstruction was again performed on a matrix of 1 mm^3 voxels. For comparison to the BPF reconstructions, the same 2D Gaussian smoothing filter was applied ($\sigma = 1/\sqrt{2}$ pixels) as a post-processing step in image-space. We note that more complex binning approaches have been suggested for FBP in proton CT (Rit *et al* 2013), but the optimal binning is still an open question and not the subject of this study.

3. Results

A central axial slice reconstruction (x-y plane) is shown in figure 3a for the BPF algorithm (9-knot path, 1.0 mm voxels, Gaussian filter). The two orthogonal planes (y-z and x-z) are shown in figures 3b and 3c. Interior elliptical regions of relative stopping-power either 1.00 or 1.03 are present and easily distinguished from the background value of 1.02. The tungsten bar is also present in 3a and 3b and resolvable. The scan (180×10^7 protons) produced an absorbed dose of 5.1 mGy at the centre of the phantom.

A non-central axial slice ($z = -2.0 \text{ cm}$) is shown in figure 4 for: (a) SFBP, (b) BPF (0-knot), (c) BPF (2-knot) and (d) BPF (9-knot) algorithms. The filtered backprojection image is severely blurred. The crudest backprojection-then-filtering approach (0-knot) is a noticeable improvement over SFBP, although some artefacts are apparent: a dark shading inside the outer high-density annulus can be seen. This error is caused by the lack of knot points paced on the surface of the phantom. Increasing the number of knots to two (entry and exit) improves the spatial resolution further and eliminates the artefact. The resolution improvement of a 9-knot spline path over 2-knot is more subtle and not readily apparent in these images (resolution is addressed further below). The standard deviations of relative stopping-power within the region-of-interest (ROI) labelled 1 in figure 4d, were 0.0066 and 0.0050, respectively, for the SFBP and BPF (9-knot) algorithms. The SFBP image therefore also manifests higher noise, as well as suffering poorer resolution.

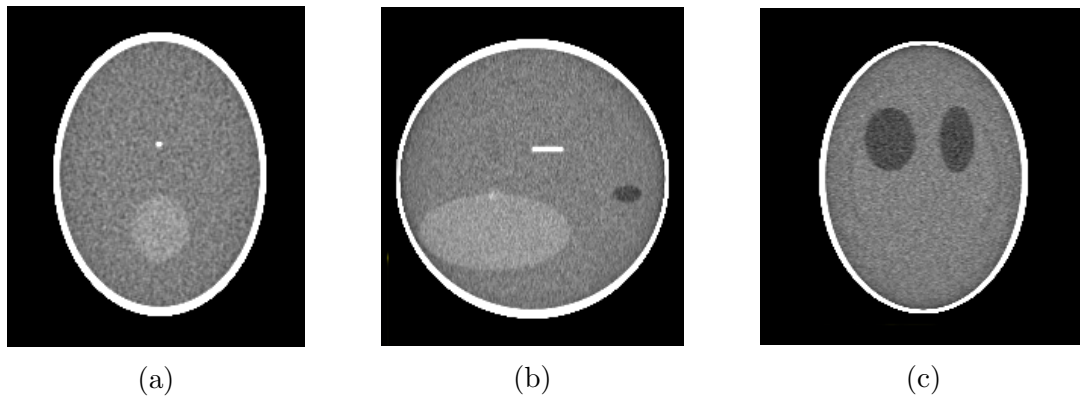


Figure 3: Central slice reconstructed using a BPF (9-knot) method for: (a) the x-y plane, (b) the z-y plane and (c) the x-z plane. Windowing selection: 0.97 to 1.07 in RSP.

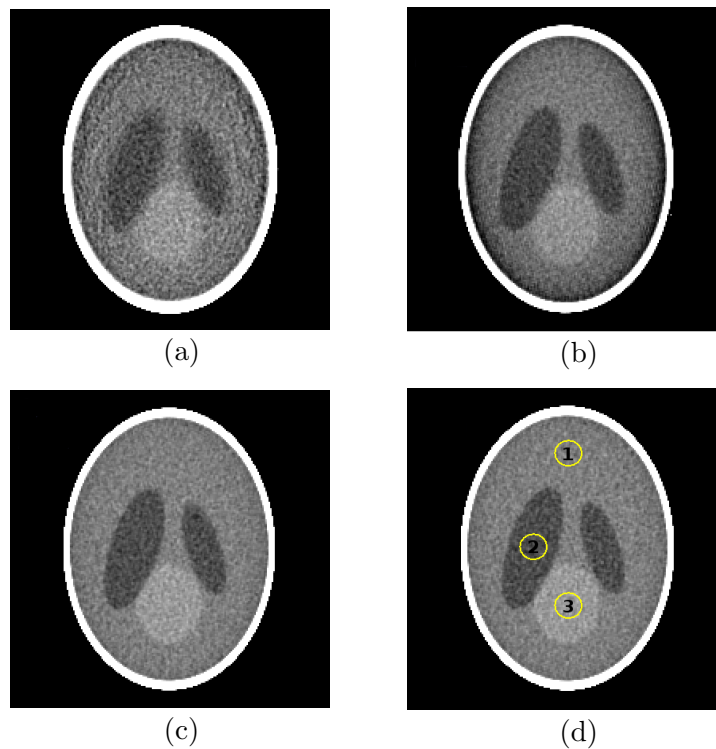


Figure 4: A transverse slice ($z=2.0$ cm, 1.0 mm voxels, Gaussian filter) reconstructed by (a) SFBP, (b) BPF (0-knot), (c) BPF (2-knot) and (d) BPF (9-knot) methods.

Regardless of general image-quality, the usefulness of the BPF algorithm will be compromised if it cannot provide quantitatively accurate reconstructions. Table 1 provides the reconstructed relative stopping-power in the three ROIs depicted in figure 3d with and without the finite matrix correction and for two different sizes of backprojection matrix. Two notable observations can be made. Firstly, as the size of the backprojection matrix is increased with respect to the reconstruction matrix, the

Table 1: Reconstructed RSP values averaged in three ROIs in comparison to true relative stopping-power. Results are given with (f_{Δ}) and without (f) finite-matrix correction and are shown for two different backprojection matrix sizes ($N = 400$ and 800). In each case the reconstruction volume was 200^3 voxels ($M=L=200$).

ROI	True RSP	N=400		N=800	
		f	f_{Δ}	f	f_{Δ}
1	1.020	1.057	1.021	1.027	1.019
2	1.000	1.035	0.999	1.008	1.000
3	1.030	1.066	1.030	1.039	1.030

uncorrected BPF algorithm becomes more accurate. This is expected. Secondly, by applying the finite matrix correction derived in this paper, an accuracy within 0.1% can be obtained even for a modestly oversized back-projection matrix ($N = 2M$). It should be noted that the reconstruction time was dominated by the backprojection step and that this increases approximately linearly with backprojection matrix size. Rates of 1.06×10^8 and 5.2×10^7 protons per hour per thread were obtained, with $N = 400$ and $N = 800$, respectively.

The resolution properties of the algorithm can be assessed from figure 5. A region around the tungsten bar is shown in the figure for the BPF algorithm ($0.5 \times 0.5 \times 1.0$ mm³ voxels, no Gaussian filter) for: (a) 0-knots, (b) 2-knots, (c) 3-knots and (d) 5-knots. An improvement in the resolution as the number of knots is increased is clear (although negligible after 5-knots and therefore not shown). The corresponding MTFs are shown in figure 6. Little improvement is seen for greater than a 3-knot proton path, although this is likely to depend on the location of the point-of-interest within a phantom and the initial energy of the proton beam.

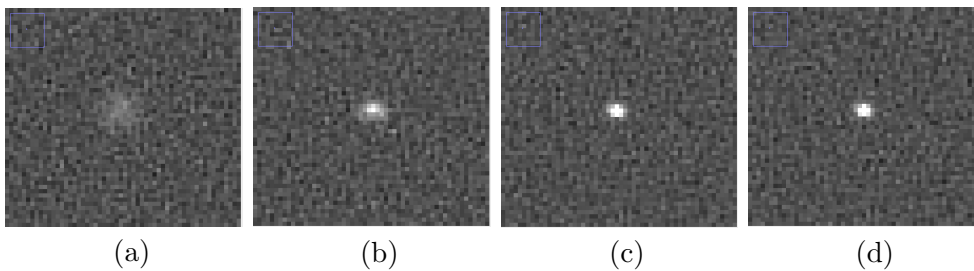


Figure 5: A zoomed-in region of a transverse slice around the tungsten rod, reconstructed with (a) 0-knot, (b) 2-knot, (c) 3-knot and (d) 5-knot proton paths.

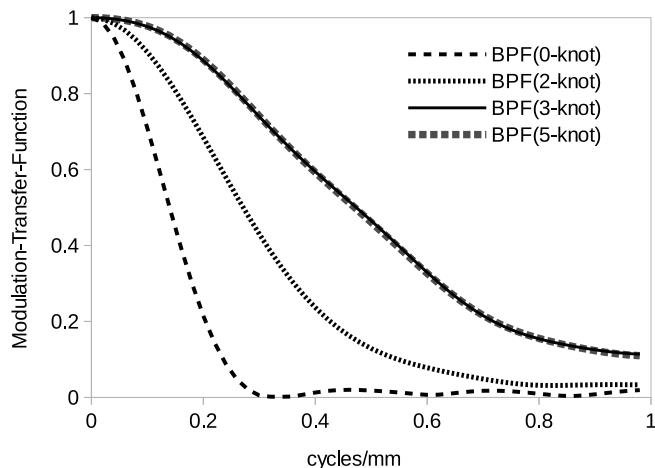


Figure 6: Modulation-Transfer-Functions calculated from the simulated data based on 0, 2, 3 and 5-knot proton path reconstructions.

4. Discussion

A new approach to proton CT reconstruction has been introduced. It has been argued that this method of backprojection-then-filtering naturally suits the nature of the problem: it is a list mode algorithm naturally accommodating non-linear paths. With the appropriate treatment of the 2D kernel and the application of a finite matrix correction derived here, a high quantitative accuracy ($\approx 0.1\%$) has been demonstrated. The superiority of the BPF method over the standard FBP, in terms of spatial resolution and noise, has been illustrated. The proposed method is less computationally demanding than an iterative or statistical reconstruction approach, which would require multiple backprojection steps. The algorithm is also highly parallelizable, lending itself to multi-threaded execution. A piece-wise linear approximation to a cubic spline proton path was applied for reconstruction. Results suggest that five interpolation knots are likely to be sufficient for practical purposes.

The use of a Monte Carlo simulation for the illustrative reconstructions here has allowed an appreciation of the fundamental limits of image-quality, deriving from proton interaction mechanisms. It should be noted, however, that perfect 4-vector information has been assumed in the entry and exit planes. This is not a realistic representation of the experimental situation where there may be substantial uncertainties on these quantities. Therefore the image-quality presented here should be interpreted as a bound on that obtainable with the same number of protons per projection, event rejection cuts, reconstruction parameters and proton path approximation. A more thorough model of a realistic system would be of interest, but as it would be system-specific, it is beyond the scope of the current work.

5. Conclusion

A new and quantitatively accurate reconstruction method for proton CT using backprojection-then-filtering has been demonstrated. The method is straight-forward to implement and possesses superior characteristics to the standard filtering-then-backprojection approach.

Acknowledgments

The authors wish to thank aSpect Systems GmbH and ISDI Limited for their support and development of the PRaVDA system. The authors further acknowledge the support and insight of the whole PRaVDA team. This work was supported by the Wellcome Trust Translation Award Scheme, Grant Number 098285.

References

- Beister M, Kolditz D and Kalender W A 2012 Iterative reconstruction methods in x-ray CT *Phys Med Biol.* 28(2) 94-108
- Berger M J, Coursey J S, Zucker M A and Chang J 2005 *ESTAR, PSTAR, and ASTAR: Computer Programs for Calculating Stopping-Power and Range Tables for Electrons, Protons, and Helium Ions (version 1.2.3)* [Online] Available: <http://physics.nist.gov/Star> [2014-05-03], National Institute of Standards and Technology, Gaithersburg, MD
- Bruzzi M, Blumenkrantz N, Feldt J, Heimann J, Sadrozinski H F-W, Seiden A, Williams D C, Bashkirov V, Schulte R, Menichelli D, Scaringella M, Cirrone G A P, Cuttone G, Randazzo N, Sipala V and Lo Presti D 2007 Prototype Tracking Studies for Proton CT *IEEE Trans. Nucl. Sci.* 54(1) 140-145
- Cirrone G A P, Bucciolini M, Bruzzi M, Candiano G, Civinini C, Cuttone G, Guarino P, Lo Presti D, Mazzaglia S E, Pallotta S, Randazzo N, Sipala V, Stancampiano C and Talamonti C 2011 Monte Carlo evaluation of the Filtered Back Projection method for image reconstruction in proton computed tomography *Nucl. Instrum. Methods A* 658 7883
- Civinini C, Brianzi M, Bruzzi M, Bucciolini M, Candiano G, Capineri L, Cirrone G A P, Cuttone G, Lo Presti D, Marrazzo L, Mazzaglia E, Menichelli D, Pieri S, Randazzo N, Sipala V, Stancampiano C, Talamonti C, Tesi M and Valentini S 2010 Towards a proton imaging system *Nucl. Instrum. and Methods A* 623 588590
- Cormack A M 1963 Representation of a Function by its Line Integrals, with Some Radiological Applications *J. Appl. Phys.* 34 2722
- Cormack A M and Koehler A M 1976 Quantitative Proton Tomography: Preliminary Experiments *Phys. Med. Biol.* 21(4) 560-569
- Ferrari A, Sala P R, Fasso A and Ranft J 2005 FLUKA: a multi-particle transport code *CERN Yellow Report CERN-2005-10, INFN/TC05/11, SLAC-R-773*.
- Hanson K M, Bradbury J N, Cannon T M, Hutson R L, Laubacher D B, Macek R, Paciotti M A and Taylor C A 1978 The Application of Protons to Computed Tomography *IEEE Trans. Nucl. Sci.* NS-25 657-660
- Hanson K M 1979 Proton computed tomography *IEEE Transactions on Nuclear Science* NS-26(1) 1635-1640
- Li T, Liang Z, Singanallur J V, Satogata T J, Williams D C, Schulte R W 2006 Reconstruction for proton computed tomography by tracing proton trajectories: a Monte Carlo study *Med Phys.* 33(3) 699-706
- Jeffrey A and Zwillinger D (eds.) 2000 *Gradshteyn and Ryzhik's Table of Integrals, Series, and Products Sixth edition* (Academic Press).

- Kak A C and Slaney M 2001 *Principles of Computerized Tomographic Imaging* (Society of Industrial and Applied Mathematics).
- Penfold S N, Rosenfeld A B, Schulte R W, Schubert K E 2009 A more accurate reconstruction system matrix for quantitative proton computed tomography *Med Phys.* 36(10) 4511-8.
- Penfold S N, Schulte R W, Censor Y, Rosenfeld A B 2010 Total variation superiorization schemes in proton computed tomography image reconstruction *Med Phys.* 37(11) 5887-95
- Poludniowski G, Allinson N M, Anaxagoras T, Esposito M, Green S, Manolopoulos S, Nieto-Camero J, Parker D J, Price T, Evans P M 2014 Proton-counting radiography for proton therapy: a proof of principle using CMOS APS technology *Phys Med Biol.* 59(11) 2569-81
- Rit S, Dedes G, Freud N, Sarrut D, Letang JM 2013 Filtered backprojection proton CT reconstruction along most likely paths *Med Phys.* 40(3) 031103
- Rosenheinrich W 2013 *Tables of Some Indefinite Integrals of Bessel Functions* available at: <http://www.fh-jena.de/rsh/Forschung/Stoer/besint.pdf>
- Sadrozinski H F-W, Johnson R P, Macafee S, Plumb A, Steinberg D, Zatserklyaniy A, Bashkirov V A, Hurley R F, Schulte R W 2013 Development of a head scanner for proton CT *Nucl. Instrum. and Methods A* 699 205210.
- Schneider U, Besserer J, Pемler P, Dellert M, Moosburger M, Pedroni E and Kaser-Hotz B 2004 First proton radiography of an animal patient *Med Phys.* 31(5) 1046-51
- Schneider U and Pedroni E 1994 Multiple Coulomb scattering and spatial resolution in proton radiography *Med Phys.* 21(11) 1657-63
- Schulte R R, Penfold S N, Tafas J T, Schubert K E 2008 A maximum likelihood proton path formalism for application in proton computed tomography *Med Phys.* 35(11) 4849-56
- Suzuki S and Yamaguchi S 1988 Comparison between an image reconstruction method of filtering backprojection and the filtered backprojection method *Applied Optics* 27(14) 2867-70
- Vlachoudis V 2009 FLAIR: a powerful user friendly graphical interface for FLUKA *International Conference on Mathematics, Computational Methods & Reactor Physics 2009 (Saratoga Springs, New York)* (Illinois, USA: American Nuclear Society).
- Wang D, Mackie T R and Tome W A 2010 On the use of a proton path probability map for proton computed tomography reconstruction *Med Phys.* 37(8) 4138-45
- Williams D C 2004 The most likely path of an energetic charged particle through a uniform medium *Phys Med Biol.* 49(13) 2899-911
- Zeng G L and Gullberg G T 1994 A backprojection filtering algorithm for a spatially varying focal length collimator *IEEE Transactions on Medical Imaging* 13(3) 549-556
- Zeng G L and Gullberg G T 1995 Can the backprojection filtering algorithm be as accurate as the filtered backprojection algorithm? *Nuclear Science Symposium and Medical Imaging Conference 1994, IEEE Conference Record Vol. 3* 1232-1236